Nuclear Instruments and Methods in Physics Research B 393 (2017) 135–139

Contents lists available at ScienceDirect

Nuclear Instruments and Methods in Physics Research B

journal homepage: www.elsevier.com/locate/nimb

Kinetic Monte Carlo simulation of phase-precipitation versus instability behavior in short period FeCr superlattices

F.J. Rodríguez-Martínez [a], J.F. Castejón-Mochón [a,*], P. Castrillo [a], R. Berenguer-Vidal [a], I. Dopico [b], I. Martin-Bragado [b]

[a] UCAM, Universidad Católica de Murcia, Campus de los Jerónimos, 30107 Guadalupe (Murcia), Spain
[b] IMDEA Materials Institute, Eric Kandel 2, 28906 Getafe (Madrid), Spain

ARTICLE INFO

Article history:
Received 1 August 2016
Received in revised form 23 September 2016
Accepted 29 September 2016
Available online 13 October 2016

Keywords:
FeCr alloys
Superlattices
Kinetic Monte Carlo
Spinodal

ABSTRACT

The structural evolution of FeCr superlattices has been studied using a quasi-atomistic Object Kinetic Monte Carlo model. Superlattices with different spatial periods have been simulated for anneal durations from few hours to several months at 500 °C. Relatively-long period superlattices stabilize into Fe-rich and Cr-rich layers with compositions close to those of bulk α and α′ phases. In contrast, superlattices with very short periods (4, 5, 6 nm) are observed to undergo instability and, for long annealing times, evolve into three-dimensionally decomposed regions, in qualitative agreement to recent experimental observations. The instability onset is delayed as the spatial period increases, and it occurs via interface roughness. This evolution can be explained as a minimization of the free-energy associated to the α/α′ interfaces. A comprehensive description of the evolution dynamics of FeCr-based structures is obtained with our model.

1. Introduction

Iron-chromium (FeCr) alloys are materials of high technological and fundamental interest [1]. From the technological point of view, they have been selected as structural materials for advanced nuclear applications [2]. From the fundamental side, they exhibit a rich phenomenology with a miscibility-gap leading to phase nucleation for moderated Cr content and spinodal decomposition for the medium composition range, and these processes are accelerated by radiation [3–5]. The composition-dependence of the alloy mixing energy has been subject of active discussions, and some uncertainties are still remaining for the phase diagram [6].

Phase decomposition in nominally homogeneous alloys is triggered by random composition fluctuations. Such phase decomposition can be also induced artificially in composition-modulated superlattices (SLs), with Fe-rich and Cr-rich regions acting as seeds for phase nucleation [7]. Thus, Fe-rich layers would precipitate into a bulk-like Fe-rich phase (α-phase) whereas Cr-rich layers would precipitate into a bulk-like Cr-rich phase (α′-phase), with metastable α/α′ interface regions [8]. In this way, the layers are expected to stabilize and the modulation amplitude of FeCr SLs may increase under anneal. This behavior is opposite to usual SL interdiffusion.

Recently, Atom Probe Tomography (APT) measurements revealed that very thin-layer FeCr SLs, with spatial period of 6 ± 1 nm, undergo instability, instead of stabilization, at 500 °C. In particular, composition profiles become irregular after few days anneals, losing the original periodicity. For longer anneals, the system is observed to evolve toward three-dimensional morphologies [9]. These results have been interpreted in terms of a critical layer thickness on the light of a one-dimensional Mean Field Model [9]. Nevertheless, it would be desirable to count on a comprehensive model including the whole phenomenology: random nucleation of homogeneous alloys, phase-stabilization of thick-layer SLs, instability for thin-enough layers, and evolution toward three-dimensional morphologies for advanced stages.

Atomistic-like Object Kinetic Monte Carlo models (OKMC) are promising candidates to simulate the structural evolution of crystal alloys, reaching the required time scales of typical experiments, while preserving a direct connection to atom-scale processes [10–12]. Recently, a defect-based OKMC model has demonstrated to provide an accurate description over time of phase nucleation and spinodal decomposition in FeCr alloys [8], while offering improved computational efficiency respect to more detailed models [13].

* Corresponding author.
E-mail address: jfcastejon@ucam.edu (J.F. Castejón-Mochón).

http://dx.doi.org/10.1016/j.nimb.2016.09.026
0168-583X/

In this work, the above mentioned OKMC model has been extended to simulate the evolution of FeCr-based SLs, including ultra-thin SLs. Our purpose is to provide a unified picture for the structural evolution of iron-chromium alloy systems, including regular phase-separation and short-period superlattice instability. The paper is organized as follows. After this introduction, the model and methods used in the simulations are sketched out. Subsequently, the simulation results are presented and the corresponding discussion is developed. Finally, some conclusions are wrapped up.

2. Model and methods

We have used the OKMC model described by *Dopico* et al. [8] and we have applied it to FeCr alloys with initial periodic one-dimensional composition modulation (FeCr superlattices, SLs). In that model, mobile point-defects are treated as atomistic particles whereas lattice atoms (Fe or Cr) are described by integer counters in each local region [10]. With this aim, the simulation domain is divided into nanometer-sized cells. Material properties in each cell are assumed to depend on its own Cr-molar fraction (composition) and on the composition of neighbor cells having atomic bonds to this, with weights derived from a simple crystallographic bond model and accounted in terms of an effective composition [8]. Composition dependence of formation energy of point-defects, migration energy of point-defects, tracer diffusivity ratio between Cr and Fe atoms, and alloy mixing energy are included in the model.

Point-defects moving from a cell to another may induce the movement of Cr or Fe atoms, with probabilities depending on the tracer diffusivity ratios and on the mixing energies of the cells. Within our model, point-defect induced atom movements are accounted by an efficient exchange algorithm. Near equilibrium conditions, point-defect concentrations depend on their formation energies. Moreover, in metals near equilibrium, vacancies are dominant over self-interstitials [14]. The model has been implemented into the MMonCa simulator [15,16].

In our simulations, the initial composition has been set to be spatially modulated in one dimension. As the model is intrinsically three-dimensional, this initial condition does not impose a constraint for the subsequent evolution. Sinusoidal Cr molar fraction profiles with amplitude of 0.25 and average of 0.5 and an anneal temperature of 500 °C have been selected to reproduce the physical conditions of the experimental measurements [9]. Different SL periods (λ) have been used with the aim of studying layer stability/instability as a function of layer thickness. A simulation domain of $12 \times 60 \times 99\ \mathrm{nm}^3$, divided in cubic cells with side $L = 0.6$ nm, has been considered. This cell side is close to the lowest limit of the approach ($L \geqslant 2a \approx 0.57$ nm, with a being the lattice parameter). A free surface has been located at the domain front (0 nm depth), mirror boundary conditions have been assumed at the bottom (99 nm depth), and periodic boundary conditions have been set in the lateral (12 nm × 60 nm) directions [8].

Equilibrium vacancy concentration (with negligible self-interstitial contribution) is assumed in our simulations. This is established by the balance of vacancy emission and capture at the free surface, and by the probability of vacancy jumps between cells [8,10]. Therefore, simulation times would match to experimental conditions with low initial defect concentration. If extra defects are in the sample, either incorporated during epitaxial growth or generated by irradiation, experimental dynamics is expected to be accelerated with regard to the predicted one. Additionally, the presence of oxygen impurities, evidenced in the experiments of Ref. [9], has not been included in our simulations. The parameter set of Ref. [8] has been used, with the vibrational entropy parameter Θ tuned from 1400 K to 1300 K in order to compensate the discrepancies of precipitate compositions in Ref. [9] with respect to the original calibration.

Spatial composition maps and profiles, suitable to be compared to APT experiments, can be extracted from the simulated composition configurations. With this aim, the alloy composition is averaged within a volume analogous to the one probed by the experimental beam. In the reference experiment, a beam spot with a diameter of 0.5 nm and a probing profundity of 8 nm has been used [9] and it can be equated to a column of 7 cubic cells for our 0.6 nm spacing. Thus, simulated composition maps (or profiles) are built by scanning the simulation domain within a cell plane

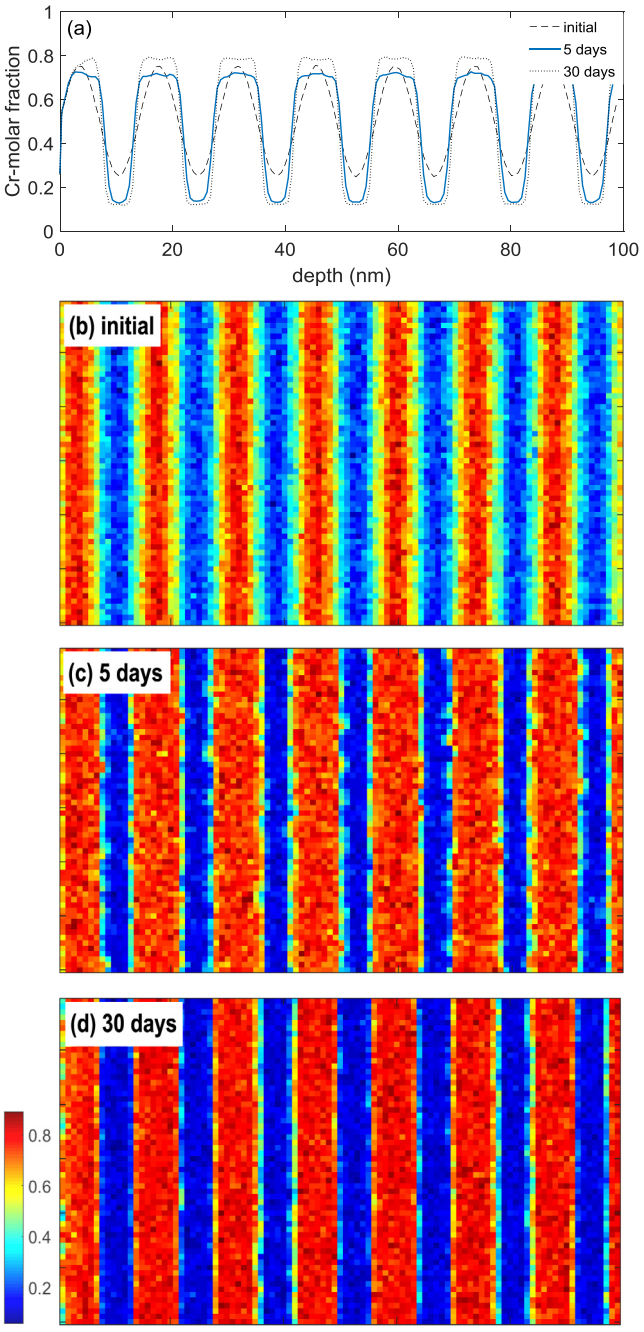

Fig. 1. Simulated spatial composition distribution, measured as Cr molar fraction, for a 14 nm-period FeCr superlattice with initial sinusoidal composition modulation annealed at 500 °C. (a) Initial and aged composition profiles. (b) Initial composition map. (c) and (d) Composition maps after annealing for 5 and 30 days, respectively.

(or row) and averaging along the corresponding probed volume in the perpendicular direction (see Fig. 1).

The mean mixing free energy per atom of the simulated domain, $\langle G_{mix}\rangle$, can be analyzed as a measure of its thermodynamic stability. It can be calculated as $\langle G_{mix}\rangle = \sum_i G_{mix_i}/N$, where N is the number of cells in the simulation and G_{mix_i} is the free mixing energy per atom in cell i, which is given by [17]:

$$G_{mix_i} = E_{mix}(x_i)\left(1-\frac{T}{\Theta}\right) + k_B T[X_i lnX_i + (1-X_i)\ln(1-X_i)] \quad (1)$$

where E_{mix} is the mixing energy at 0 K, T is the absolute temperature, k_B is the Boltzmann constant, and x_i and X_i are the effective and unweighted Cr fraction of cell i, respectively [8]. The composition of α and α' phases are those minimizing the mean mixing free energy at a given temperature in a bulk system (i. e., when no interfaces are considered).

3. Simulation results

Fig. 1 displays the simulation results for a FeCr SL with initial composition modulated in depth between 0.25 and 0.75 Cr molar fraction with a period of $\lambda = 14$ nm. This period is much longer than the 6 ± 1 nm period for which instability was experimentally observed. An anneal at 500 °C up to 30 days has been simulated. The composition profile is observed to evolve from a sinusoidal shape toward a square-wave shape (Fig. 1a), with iron-rich regions precipitating to α-phase and chromium-rich regions precipitating to α′-phase. For 30 days anneal, the Cr molar fraction in the plateaus of the profile is stabilized near the concentration values analytically predicted for bulk phases. Fig. 1b–d display the evolution of the two-dimensional composition map. Besides the formation of uniform α and α′ domains, the interfaces between α and α′ domains are observed to narrow and flatten.

In order to analyze the SL behavior for lower periods, a sample with three different regions, initially with periods of $\lambda = 5$, 4, and 6 nm, and an anneal temperature of 500 °C has been considered in the simulations of Fig. 2. After 4 days anneal (Fig. 2a) the region of shortest period ($\lambda = 4$ nm) exhibits features of instability, with a trend dramatically different to the one observed in Fig. 1 for $\lambda = 14$ nm. Rather, this resembles the instability behavior observed in the experiments for $\lambda = 6 \pm 1$ nm with irregular modifications of the concentration profile [9]. However, in contrast to the referenced experiment, no clear amplitude conservation occurs in most periods of the $\lambda = 4$ nm simulated region. For longer anneals the one-dimensional modulation with 4 nm period is erased and a three-dimensional pattern is spontaneously formed in its place, as it can be seen for 15 days in Fig. 2b.2. For even longer anneals (Fig. 2c), this gives rise to a vein-like three-dimensional morphology, similar to the one resulting from the spinodal decomposition of homogeneous alloys [8].

A delay of the instability onset, respect to the one for $\lambda = 4$ nm, is found in the simulations for the region with spatial period of $\lambda = 5$ nm. In this region, the wavy character of the initial modulation is preserved for 4 and for 15 days anneals, as it can be seen in Fig. 2a.1 and b.1. For these aging times, the concentration maxima hardly increase whereas the initial minima decrease, very much in agreement to the profile shape in the initial stages of the experiment for $\lambda = 6$ nm [9]. For 15 days, a development of interface roughness is observed in Fig. 2b.2, causing modulation irregularities in local areas. For longer times, the interface roughness increases, coming to bridge contiguous Cr-rich (or Fe-rich) planar precipitate layers. Once a number of local bridges are formed, the precipitates evolve toward three-dimensional morphologies (see Fig. 2c, for 75 days anneal), analogous to those of the $\lambda = 4$ nm region and in qualitative agreement to the experiment.

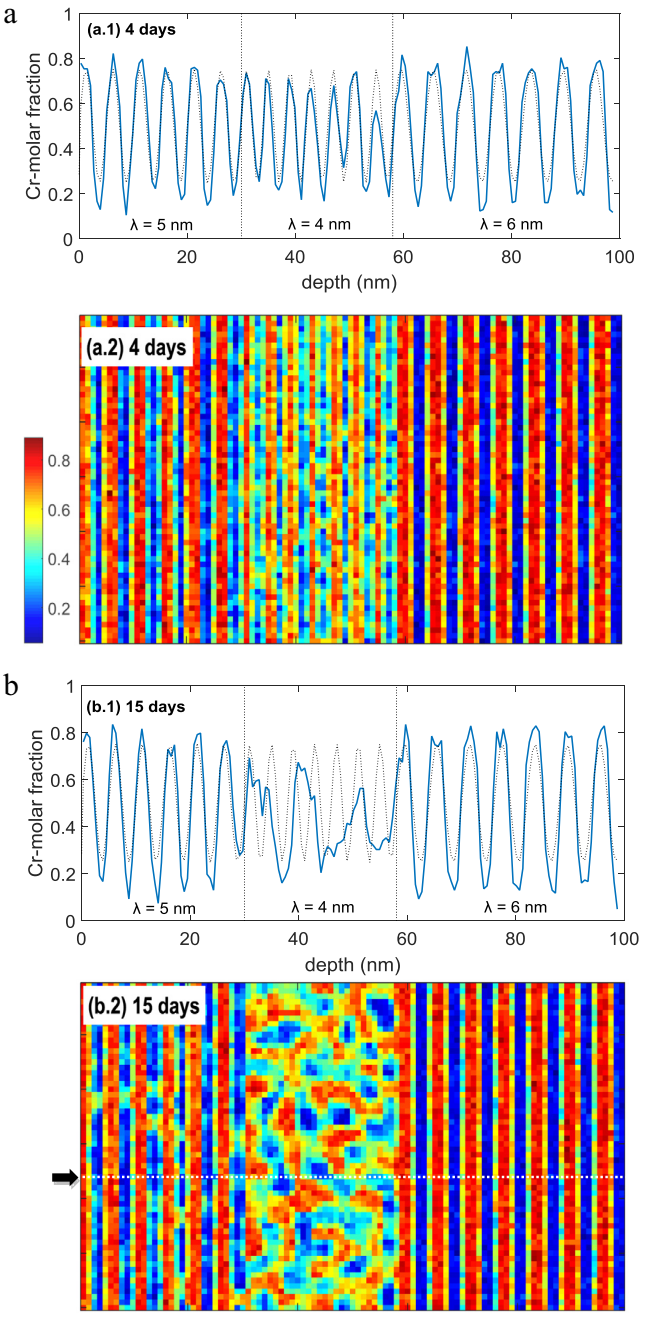

Fig. 2. Simulated spatial composition distribution for a FeCr structure formed by three regions with initial sinusoidal modulation of (from left to right) 5, 4, and 6 nm periods annealed at 500 °C during (a) 4 days, (b) 15 days, and (c) 75 days. A composition profile (subpanel 1) and a composition color map (subpanel 2) are displayed in each case. (The composition profile was recorded along the dotted white line marked on the map).

Concerning the $\lambda = 6$ nm region, it behaves in the middle way between the $\lambda = 5$ nm region and the $\lambda = 14$ nm SL. In this case, the modulation amplitude slightly increases for 4 and 15 days aging times and the concentration maxima and minima reach values close to those of α and α′ phases, although no clear plateaus are observed in the profiles (Fig. 2a and b). For longer anneal time, even this region exhibits roughness (Fig. 2c.2), preluding instability for long enough anneals. The discrepancies between the simulations in this region and the experiment for $\lambda = 6$ nm will be discussed in next section.

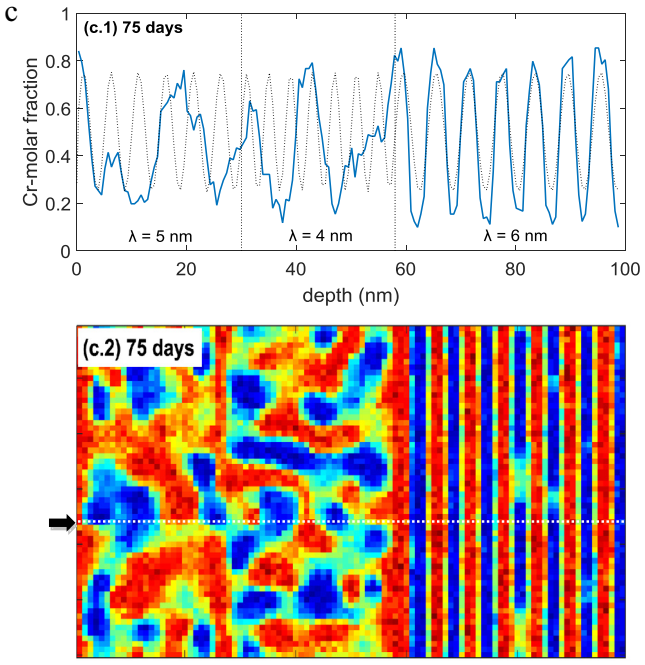

Fig. 2 (*continued*)

The different behavior of short- and "long"-period SLs can be explained in terms of mixing free energy minimization, as a driving force for system evolution. For relatively-long period SLs (as the $\lambda = 4$ nm SL of Fig. 1), the formation of planar bulk-like phases (where G_{mix} is minimized), together with the decrease of the volume of α/α' interface regions (where G_{mix} is high), constitute an efficient path to reduce $\langle G_{mix} \rangle$. The time evolution of $\langle G_{mix} \rangle$ at 500 °C for the simulations of Fig. 1 with $\lambda = 4$ nm is depicted in Fig. 3.

Specific simulations with unique period of 4 nm, 5 nm, and 6 nm have been run to evaluate $\langle G_{mix} \rangle$ for these λ values. For $\lambda = 6$ nm, the simulated evolution looks qualitatively analogous to the one of $\lambda = 14$ nm (see Fig. 3), with $\langle G_{mix} \rangle$ quickly decreasing and stabilizing, corresponding to the formation of a planar structure similar to the one observed at the 6 nm region in Fig. 2. The higher stabilized $\langle G_{mix} \rangle$ value of the 6 nm curve, compared to the 14 nm curve, is explained by its higher number of α/α' interfaces, whereas its faster initial slope can be related to the higher composition gradients in this shorter period SL, causing higher atom fluxes.

For $\lambda = 5$ nm, $\langle G_{mix} \rangle$ experiences also a decrease and stabilization for early stages, with an even higher steady value. Nevertheless, its initial evolution is slower than in the 6 nm case, consistently with the partial inhibition of precipitation observed in Fig. 2 for 5 nm modulation. Additionally, an inflexion point occurs at ~24 days, and a decrease starts to show up. This time coincides with the full development of bridges connecting planar precipitates and the beginning of the evolution toward three-dimensional shapes.

A quite different trend is followed by the curve of the 4 nm-period SL, which hardly decreases at the initial stages, exhibits a plateau up to ~7 days, and quickly decreases after ~10 days, eventually stabilizing for long term anneals. The weak initial decrease corresponds to an almost completed inhibition of one-dimensional phase formation due to the high relative volume of interface regions. The subsequent plateau is actually associated to the structural evolution from the one-dimensional modulated structure to the onset of three-dimensional precipitation, keeping

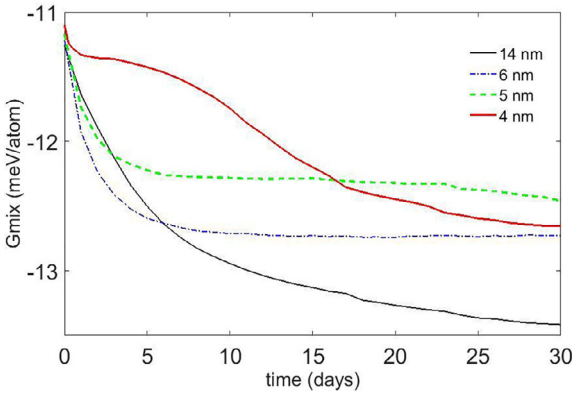

Fig. 3. Mean mixing free energy of the system, in meV per atom, as a function of anneal time at 500 °C for FeCr SLs with periods of 4, 5, 6, and 14 nm, simulated by OKMC.

almost constant $\langle G_{mix} \rangle$. Once the three-dimensional precipitates are seeded, the remarkable drop of $\langle G_{mix} \rangle$ observed after 10 days is related to the growth of these precipitates. This can be correlated to the decrease observed after ~24 days in the 5 nm-SL curve, although in that case the growth of three-dimensional precipitates can be seen as a reshape of the already formed one-dimensional precipitates.

The metastability of the 5 nm period region is revealed in Fig. 3 where the curve for $\lambda = 5$ nm is overtaken by the 4 nm curve, bringing to light that a better minimization of $\langle G_{mix} \rangle$ would be possible and, thus, announcing a possible instability for longer anneal times. Also the 6 nm curve behaves in this way, but out of the scale of Fig. 3 (see Fig. 2c.2, for 75 days, where some local instabilities are observed). We must note that, actually, even the 14 nm-period SL after 30 days (see Figs. 1d and Fig. 3) is a metastable system. In fact, the absolute minimum energy structure would be formed by two bulk-like domains with only one α/α' interface with minimum area. Hence, all the other configurations are metastable, although no evolution toward that structure will be observed for realistic aging times.

4. Discussion

The above presented OKMC simulations qualitatively reproduce, although with quantitative discrepancies, some of the recent experimental observations, together with the previously established phenomenology for the FeCr alloy system. In particular, the model correctly predicts, starting from an atom-scale basis, the modulation instability for ultra-short SLs and the stabilization to α and α' phase layers for longer period SLs. The simulated asymmetric profiles with near kinetic stasis for $\lambda = 5$ nm simulations are also in accordance with the APT profiles. Besides, the evolution of the 4 and 5 nm regions towards three-dimensional patterns for long anneal times is also reproduced and it easily links to the behavior of spinodally decomposed homogeneous alloys.

Additionally to the agreement, the model provides some insight on the structural evolution of FeCr SLs. For example, our simulations suggest that layer instability is gradually delayed with layer thickness, rather than suggesting the existence of an abrupt critical thickness independent on the anneal duration. Simulations also reveal the role of roughness in the onset of instability. Furthermore, our analysis points out that the different morphological evolution patterns can be seen as alternative ways for α/α' interface region reduction and, in turn, free-energy minimization.

However, clear quantitative discrepancies between our simulations and the published experiment [9] are observed, although only few experimental profiles have been reported up to date and no

statistical information about them is available. On one hand, the experimental onset for instability was reported to occur after an aging time of $t = 1$ day for a modulation period of $\lambda = 6 \pm 1$ nm. On the other hand, first local instabilities can be detected in simulated profiles (not shown here) at $t = 2$ days for $\lambda = 4$ nm, $t = 5$ days for $\lambda = 5$ nm, and $t = 60$ days for $\lambda = 6$ nm. Generalized instabilities are not obtained in the simulations until $t = 4$ days for $\lambda = 4$ nm and more than 15 days for $\lambda = 5$ nm. Moreover, three-dimensional pattern formation was detected in the experiment between 4 and 7 days whereas it occurs in the simulation in about one week for $\lambda = 4$ nm, in about one month for $\lambda = 5$ nm, and it is expected to appear within the time-scale of several months for $\lambda = 6$ nm. Additionally, the nearly kinetic stasis experimentally reported for $\lambda = 6 \pm 1$ nm may correspond to the simulated behavior for $\lambda = 5$ nm, whereas decreasing and increasing trends are insinuated in the simulated modulation amplitude for $\lambda = 4$ nm and $\lambda = 6$ nm, respectively.

The quantitative discrepancies between simulated and experimental data can be seen as a shift in t and/or in λ, and they could be tentatively attributed to different causes. Firstly, one possible reason could be the simplicity of the inter-cell interaction within our OKMC model [8]. Within this framework, the energy excess at α/α' interfaces (and, consequently, the instability of the structure) is assessed by means of inter-cell interaction. Therefore, the simplifications assumed in the model for inter-cell interaction could be the origin of a shift in the SL period λ at which the onset instability would be produced for a given aging time. Another possible origin could be the presence of non-equilibrium defect concentration in the experimental samples, related to defective epitaxial growth. This would result in an accelerated kinetics of the experiments respect to the simulations and, thus, in a shift on the time scale of SL evolution for a given λ. Experimental period fluctuations, quantified as ±1 nm, can also play a role. Other possible sources of discrepancies, such as the effect of the oxygen concentration in sample ($\sim$3%) cannot be excluded but are difficult to quantify.

The simulation method reported here can be extended to the study of FeCr SLs under irradiation, both at ambient temperature and at annealing temperatures. To do that, defect cascades generated by single electrons or single ions would be computed offline and loaded by the OKMC simulator, with intervals between cascades according to the dose rate. In particular, electron and irradiations at anneal temperatures, producing diluted distributions of self-interstitials and vacancies with reduced defect clustering, are expected to result in SL evolutions analogous to those obtained for equilibrium vacancy concentration but accelerated in time.

5. Conclusions

A quasi-atomistic OKMC model, originally developed for the simulation of initially homogeneous FeCr alloys has been successfully applied to simulate the structural evolution of FeCr SLs at 500 °C. A variety of evolution regimes has been identified depending on the period of the SLs and on the duration of the anneal. In particular, precipitation toward bulk-like α and α' phases has been observed for "long"-period SLs whereas instability and kinetic stasis have been obtained for ultra-short-period SLs, in agreement to the recent experimental observations. The aging time at which the instability onset is produced depends gradually on the SL period. Long-term evolution of instable ultra-short-period FeCr SLs is quite similar to the evolution of spinodally decomposed FeCr alloys. The different evolution behaviors are explained as paths for free-energy minimization. Finally, the possible sources of the quantitative discrepancies between the simulations and the experiment reported in the literature have been discussed.

Acknowledgements

This research was supported by the Fundación Seneca – Agencia Regional de Ciencia y Tecnología de la Región de Murcia (Programa de Apoyo a la Investigación) under grant 19366/PI/14.

References

[1] F.A. Garner, M.B. Toloczko, B.H. Sencer, Comparison of swelling and irradiation creep behavior of fcc-austenitic and bcc-ferritic/martensitic alloys at high neutron exposure, J. Nucl. Mater. 276 (2000) 123–142, http://dx.doi.org/10.1016/S0022-3115(99)00225-1.
[2] S.L. Dudarev et al., The EU programme for modelling radiation effects in fusion reactor materials: an overview of recent advances and future goals, J. Nucl. Mater. 386–388 (2009) 1–7, http://dx.doi.org/10.1016/j.jnucmat.2008.12.301.
[3] A. Caro, M. Caro, P. Klaver, B. Sadigh, E.M. Lopasso, S.G. Srinivasan, The computational modeling of alloys at the atomic scale: from ab initio and thermodynamics to radiation-induced heterogeneous precipitation, J. Mater. 59 (2007) 52–57, http://dx.doi.org/10.1007/s11837-007-0055-y.
[4] M. Bachhav, G. Robert Odette, E.A. Marquis, α' precipitation in neutron-irradiated Fe–Cr alloys, Scr. Mater. 74 (2014) 48–51, http://dx.doi.org/10.1016/j.scriptamat.2013.10.001.
[5] O. Tissot, C. Pareige, E. Meslin, B. Decamps, J. Henry, Kinetics of α' precipitation in an electron-irradiated Fe15Cr alloy, Scr. Mater. 122 (2016) 31–35, http://dx.doi.org/10.1016/j.scriptamat.2016.05.021.
[6] L. Malerba, G. Bonny, D. Terentyev, E.E. Zhurkin, M. Hou, K. Vörtler, K. Nordlund, Microchemical effects in irradiated Fe–Cr alloys as revealed by atomistic simulation, J. Nucl. Mater. 442 (2013) 486–498, http://dx.doi.org/10.1016/j.jnucmat.2012.12.038.
[7] T. Tsakalakos, Composition-modulated films: New materials for studying stability and critical phenomena in solid solutions, Thin Solid Films 86 (1) (1981) 79–90, http://dx.doi.org/10.1016/0040-6090(81)90161-9.
[8] I. Dopico, P. Castrillo, I. Martin-Bragado, Quasi-atomistic modeling of the microstructure evolution in binary alloys and its application to the FeCr case, Acta Mater. 95 (2015) 324–334, http://dx.doi.org/10.1016/j.actamat.2015.05.040.
[9] P. Maugis, Y. Colignon, D. Mangelinck, K. Hoummada, Spinodal decomposition in multilayered Fe-Cr system: kinetic stasis and wave instability, JOM 67 (2015) 2202–2207, http://dx.doi.org/10.1007/s11837-015-1558-6.
[10] P. Castrillo, R. Pinacho, M. Jaraiz, J. Rubio, Physical modeling and implementation scheme of native defect diffusion and interdiffusion in SiGe heterostructures for atomistic process simulation, J. Appl. Phys. 109 (2011) 103502, http://dx.doi.org/10.1063/1.3581113.
[11] T. Garnier, M. Nastar, Coarse-grained kinetic Monte Carlo simulation of diffusion in alloys, Phys. Rev. B 88 (2013) 134207, http://dx.doi.org/10.1103/PhysRevB.88.134207.
[12] M.J. Caturla, M.J. Aliaga, I. Martin-Bragado, I. Dopico, L. Malerba, M. Hernandez-Mayoral, Microstructure evolution in Fe and Fe-Cr alloys with OKMC methods, EPJ Web Conf. 115 (2016) 03001, http://dx.doi.org/10.1051/epjconf/201611503001.
[13] E. Martínez, O. Senninger, C.C. Fu, F. Soisson, Decomposition kinetics of Fe-Cr solid solutions during thermal aging, Phys. Rev. B 86 (2012) 224109, http://dx.doi.org/10.1103/PhysRevB.86.224109.
[14] H. Mehrer, N. Stolica, N. Stolwijk, Diffusion in Solids, Springer, 2007.
[15] MMonCa simulator. http://www.materials.imdea.org/MMonCa.
[16] I. Martin-Bragado, A. Rivera, G. Valles, J. Gomez-Selles, M. Caturla, MMonCa: an object kinetic Monte Carlo simulator for damage irradiation evolution and defect diffusion, Comput. Phys. Commun. 184 (2013) 2703–2710, http://dx.doi.org/10.1016/j.cpc.2013.07.011.
[17] J.M. Philibert, Atom Movements-Diffusion and Mass Transport in Solids, EDP Sciences, 2012.